Geosci. Model Dev. Discuss., 7, 3575–3593, 2014
www.geosci-model-dev-discuss.net/7/3575/2014/
doi:10.5194/gmdd-7-3575-2014


Geoscientific Model Development Discussions
Open Access



# Sensitivity of simulated $CO_2$ concentration to regridding of global fossil fuel $CO_2$ emissions

**X. Zhang[1], K. R. Gurney[1,2], P. Rayner[3], Y. Liu[4], and S. Asefi-Najafabady[1]**

[1]School of Life Sciences, Arizona State University, Tempe, AZ 85287, USA
[2]Global Institute of Sustainability, Arizona State University, Tempe, AZ 85287, USA
[3]School of Earth Sciences, University of Melbourne, 3010, Vic, Australia
[4]Laboratory for Atmosphere, Science Systems and Applications, Inc., NASA Goddard Space Flight Center Code 614 Greenbelt, MD 20771, USA

Received: 13 March 2014 – Accepted: 5 May 2014 – Published: 3 June 2014

Correspondence to: X. Zhang (tyouxia@gmail.com)

Published by Copernicus Publications on behalf of the European Geosciences Union.







## Abstract

Errors in the specification or utilization of fossil fuel $CO_2$ emissions within carbon budget or atmospheric $CO_2$ inverse studies can alias the estimation of biospheric and oceanic carbon exchange. A key component in the simulation of $CO_2$ concentrations arising from fossil fuel emissions is the spatial distribution of the emission near coastlines. Finite grid resolution can give rise to mismatches between the emissions and simulated atmospheric dynamics which differ over land or water. We test these mismatches by examining simulated global atmospheric $CO_2$ concentration driven by two different approaches to regridding fossil fuel $CO_2$ emissions. The two approaches are: (1) a commonly-used method that allocates emissions to gridcells with no attempt to ensure dynamical consistency with atmospheric transport; (2) an improved method that reallocates emissions to gridcells to ensure dynamically consistent results. Results show large spatial and temporal differences in the simulated $CO_2$ concentration when comparing these two approaches. The emissions difference ranges from $-30.3\,\mathrm{Tg\,C\,gridcell^{-1}\,yr^{-1}}$ ($-3.39\,\mathrm{kg\,C\,m^{-2}\,yr^{-1}}$) to $+30.0\,\mathrm{Tg\,C\,gridcell^{-1}\,yr^{-1}}$ ($+2.6\,\mathrm{kg\,C\,m^{-2}\,yr^{-1}}$) along coastal margins. Maximum simulated annual mean $CO_2$ concentration differences at the surface exceed ±6 ppm at various locations and times. Examination of the current $CO_2$ monitoring locations during the local afternoon, consistent with inversion modeling system sampling and measurement protocols, finds maximum hourly differences at 38 stations exceed ±0.10 ppm with individual station differences exceeding −32 ppm. The differences implied by not accounting for this dynamical consistency problem are largest at monitoring sites proximal to large coastal urban areas and point sources. These results suggest that studies comparing simulated to observed atmospheric $CO_2$ concentration, such as atmospheric $CO_2$ inversions, must take measures to correct for this potential problem and ensure flux and dynamical consistency.






GMDD
7, 3575–3593, 2014



## 1 Introduction

The terrestrial biosphere and oceans play a critical role in the global carbon cycle by removing approximately 5.1 Pg C $yr^{-1}$ of $CO_2$ out of the total emitted due to industrial activity and deforestation (Le Quéré et al., 2013). Quantification of the spatial and temporal patterns of this removal using atmospheric $CO_2$ inversions is an important approach for understanding the feedbacks between the carbon cycle and the climate system (e.g., Gurney et al., 2002). Atmospheric $CO_2$ inversions infer the ocean and biosphere uptake by solving a set of source–receptor relationships, with the fossil fuel $CO_2$ emissions acting as either a boundary condition with no uncertainty or as a "prior" flux for which some adjustment is allowed in the inversion process (Enting, 2002).

Global fossil fuel $CO_2$ emission data products are now being produced at spatial resolutions smaller than 10 km and time resolutions that resolve the diurnal cycle (Rayner et al., 2010; Oda and Maksyutov, 2011; Wang et al., 2013; Nassar et al., 2013). This, along with the increasing density of atmospheric $CO_2$ concentration observations, places new emphasis on a careful examination of the use and uncertainty associated with these high resolution fossil fuel $CO_2$ emission data products (Ciais et al., 2009; Gurney et al., 2005; Peylin et al., 2011; Nassar et al., 2013; Asefi-Najafabady et al., 2014). For example, Gurney et al. (2005) found a monthly regional bias of up to 50 % in the biosphere's net carbon exchange caused by unaccounted variation in fossil fuel emissions. Peylin et al. (2013) also showed a large response in simulated $CO_2$ concentration to the spatial and temporal resolution of fossil fuel emissions over Europe. Similarly, Nassar et al. (2013) confirmed the importance of hourly and weekly cycles in fossil fuel emissions to simulated $CO_2$ concentration levels. It is clear from these studies that the specification of the fossil fuel $CO_2$ emissions is a critical component in efforts that either use fossil fuel emissions directly or as part of an atmospheric $CO_2$ inversion process.

In addition to concerns regarding the accuracy of the high resolution fossil fuel $CO_2$ emission data products, there are elements of uncertainty in how they are used within





GMDD
7, 3575–3593, 2014



atmospheric tracer transport schemes, either in forward simulation mode or inverse mode. For example, modeled atmospheric transport processes rely on a variety of pathways, such as mixing with the planetary boundary layer, convection synoptic flow, and general circulation. Dynamical inconsistencies between these mechanisms and surface $CO_2$ fluxes, might occur with the misplacement of fossil fuel $CO_2$ emissions near coastlines or near strong urban-rural gradients where both emissions and atmospheric transport processes are changing rapidly in space. Such inconsistencies can give rise to biased results. Tracer transport models usually designate a model grid box as land vs. water, or as urban vs. rural. Typically, the choice is based on the area fractions of the underlying geography. Global tracer transport models usually run at lower resolution than the fossil fuel $CO_2$ emission data products produced in recent years and, thus, the emissions need to be aggregated to a coarser model gridcell. The aggregation process often results in water gridcells with emissions, due to instances where the minority land geography dictates a water gridcell but with the presence of emissions. The result is a water gridcell, with its accompanying ocean or lake transport dynamics, containing land emissions. This inconsistency between the emissions and transport dynamics can cause bias both locally and downwind of the errant gridcell(s). This problem is particularly important for fossil fuel $CO_2$ emissions as they are notoriously large along coastal margins where population and infrastructure are dominant.

This study aims to quantify this bias arising from the regridding of fossil fuel $CO_2$ emissions in global tracer transport simulations. We do this by constructing two experiments: (1) using the typical regridding procedure in which emissions are left in gridcells defined by the majority surface geography and (2) proportionally shifting or "shuffling" these emissions to neighboring land gridcells to maintain the spatial integrity of the fossil fuel emissions while avoiding the emissions-transport inconsistency.

Although a similar phenomenon might be expected for inland urban areas where designation of urban vs. rural gridcells may not align with surface emissions, the global tracer transport models used in this study do not attempt to resolve transport dynamics





GMDD
7, 3575–3593, 2014



over urban vs. rural areas. Thus, we restrict ourselves to the study of the land vs. water misallocation problem.

Section 2 describes the fossil fuel $CO_2$ emission data product used in the simulations, the atmospheric transport model employed and the adjustment method used the regridded emissions. Section 3 presents results highlighting the difference induced by the shuffling procedure. We examine differences in emissions and in concentrations, the latter performed at active $CO_2$ monitoring locations for which the shuffling influence is greatest. Section 4 presents our conclusions.

## 2 Methods

The impact of fossil fuel $CO_2$ emission regridding is tested here by examination of simulated $CO_2$ concentration driven by two different emission fields through an atmospheric transport model. The fossil fuel $CO_2$ emissions are aggregated from a $0.1^\circ \times 0.1^\circ$ grid to a $1.25^\circ \times 1.0^\circ$ transport model grid. One of these emission fields has the coastal gridcells "shuffled" to correct for the regridding impact ("experiment") while the other is left in the original unshuffled condition ("control").

### 2.1 Fossil fuel $CO_2$ emissions

Fossil fuel $CO_2$ emissions from the Fossil Fuel Data Assimilation System (FFDAS) version 2.0 are used as the fossil fuel $CO_2$ emissions in this study (Asefi-Najafabady et al., 2014). The FFDAS emissions are produced on a $0.1^\circ \times 0.1^\circ$ grid for every year spanning the 1997 to 2010 time period. We use emissions for 2002 in this study. The FFDAS is a data assimilation system that estimates the fossil fuel $CO_2$ emissions at every gridcell by solving a diagnostic model constrained by a series of spatially explicit observation datasets. The diagnostic model is the Kaya identity (Rayner et al., 2010) which decomposes emissions into population, economics, energy and carbon intensity terms. In FFDAS v2.0 the observational datasets are used to constrain elements in the





GMDD
7, 3575–3593, 2014



Kaya decomposition. The FFDAS uses the remote sensing-based nighttime lights data product, gridded population and national sector-based fossil fuel $CO_2$ emissions from the International Energy Agency (IEA), and a recently constructed database of global power plant $CO_2$ emissions (Elvidge et al., 2009; Asefi-Najafabady et al., 2014; Gurney and Coltin, 2014).

## 2.2 Atmospheric transport model

This study uses a global tracer transport model, the Parameterized Chemical Transport Model (PCTM) to simulate the $CO_2$ concentration resulting from the FFDAS surface emissions (Kawa et al., 2004, 2010). The model uses dynamical fields from the Modern-Era Retrospective analysis for Research and Applications (MERRA) (Bosilovich, 2013), which is a NASA reanalysis for the satellite era using a new version of the Goddard Earth Observing System Data Assimilation System Version 5 (GEOS-5). The model uses a semi-Lagrangian advection scheme; the subgrid-scale transport includes convection and boundary layer turbulence processes. The model is run at 1.25° longitude × 1.0° latitude with 56 hybrid vertical levels.

The simulation is run for four years, driven by 2002 MERRA meteorology and fossil fuel $CO_2$ surface emissions (cycled repeatedly). The MERRA meteorology has a 3 h time resolution and a 7.5 min time step is used in the model simulations. There is no time structure in the fossil fuel emissions. The first three-year period is used for spin-up and the last year is used for analysis. The PCTM outputs hourly $CO_2$ concentration at every point in the three-dimensional grid. The annual mean surface $CO_2$ concentration field and hourly time series at GLOBALVIEW-$CO_2$ monitoring sites are analyzed (http://www.esrl.noaa.gov/gmd/ccgg/globalview/co2/co2_observations.html) (Masarie and Tans, 1995).





GMDD
7, 3575–3593, 2014



### 2.3 Coastal "shuffling"

The FFDAS emissions are regridded from the original $0.1^\circ \times 0.1^\circ$ resolution to the $1.25^\circ \times 1.0^\circ$ resolution of the PCTM. The two grids have the same origin and hence, the coarser grid is overlaid onto the finer grid and the $0.1^\circ$ gridcells are integrated, as needed. In the longitudinal direction, gridcell boundaries do not align and so area-weighting was used to distribute emissions.

The PCTM utilizes a gridded land/sea mask that is used to denote the character of the model surface (land vs. ocean/lake). The designation is based on what constitutes the majority type within each gridcell. In order to maintain dynamical consistency with the land/sea mask, those gridcells that are considered ocean/lake by the mask but contain emissions integrated from the $0.1^\circ$ degree emissions grid, are treated with a "shuffling" procedure. These gridcells will have the emitted quantities transferred to adjacent land gridcells according to weights assigned by the relative magnitude of those adjacent land gridcells (see Fig. 1). The weight is defined as the ratio of emissions in each of the designated adjacent gridcells to the sum of their emissions:

$$W_j = F_j \Big/ \sum_{i=1}^{N} F_i \tag{1}$$

where $W_j$ is the weight of the $j$th land gridcell, $F_j$ is its emissions, $N$ is the total number of land gridcells to which emissions are transferred. Adjacent gridcells are defined as those sharing a border or whose corners intersect at a corner.

## 3 Results and discussion

### 3.1 Emissions difference

The shuffling procedure reallocates emissions along global coastlines but the impact on the final $CO_2$ fluxes is most pronounced where there are large coastal emissions





GMDD
7, 3575–3593, 2014



associated with urban areas or large point sources. Figure 2 shows the difference in surface emissions between the control and experiment emissions fields. The coastal locations with cities or large point sources exhibit an emissions "dipole". Positive values reflect the addition of emissions to land gridcells adjacent to those designated as ocean in the coarse grid land/sea mask while negative values reflect the removal of emissions from gridcells designated as ocean.

The largest emissions adjustments occur in coastal areas of the US Great Lakes, coastal Europe, China, India and Japan. The range of the emission difference varies from $-30.3\,\mathrm{Tg\,C\,gridcell^{-1}\,yr^{-1}}$ ($-3.39\,\mathrm{kg\,C\,m^{-2}\,yr^{-1}}$) to $+30.0\,\mathrm{Tg\,C\,gridcell^{-1}\,yr^{-1}}$ ($+2.6\,\mathrm{kg\,C\,m^{-2}\,yr^{-1}}$). To provide context, an emission difference of $30\,\mathrm{Tg\,C\,gridcell^{-1}\,yr^{-1}}$ is equivalent to ~ 62 % and ~ 13 % of the annual total carbon emissions for the Netherlands and Germany in 2002, respectively, but is only limited to a few gridcells in Eastern Asia. Most emission differences in land gridcells vary in between $0.001\,\mathrm{Tg\,C\,gridcell^{-1}\,yr^{-1}}$ ($0.0001\,\mathrm{kg\,C\,m^{-2}\,yr^{-1}}$) and $5.0\,\mathrm{Tg\,C\,gridcell^{-1}\,yr^{-1}}$ ($0.056\,\mathrm{kg\,C\,m^{-2}\,yr^{-1}}$). The summed magnitude of the emissions that are relocated from ocean to neighboring land gridcells is $674.5\,\mathrm{Tg\,C\,yr^{-1}}$, which is equivalent to ~ 10 % of the global total fossil fuel $CO_2$ emissions in 2002.

### 3.2 $CO_2$ concentration difference

The atmospheric $CO_2$ concentration resulting from the control and experiment simulations offers additional insight into the impact of the regridding and coastal shuffling (Fig. 3). Similar to the emissions difference, the simulated $CO_2$ concentrations in the lowest model layer show differences along coastlines where large urban centers or point sources are present. In contrast to the emission differences, the response of surface $CO_2$ concentration not only reflects the immediate local emission impact but also a downwind impact as the differing concentration fields are transported by atmospheric motion. A particularly notable example is the surface $CO_2$ concentration difference downwind of the cluster of large coastal western European cities, for example, London, Rotterdam, Groningen, Barcelona and Rome. Also evident are dipole patterns





GMDD
7, 3575–3593, 2014



associated with many of the large $CO_2$ concentration differences along the coastline driven by the emission dipole explained in Sect. 3.1, with negative values over ocean gridcells and positive values over the adjacent land gridcells.

The annual mean concentration differences range from −6.60 ppm to +6.54 ppm at the gridcell scale. These $CO_2$ concentration differences should be placed in the context of well-known surface concentration gradients such as the north-south gradient in annual mean $CO_2$ concentration of ∼ 4.0 ppm and Northern Hemisphere longitudinal gradients of ∼ 1.5 ppm (Conway and Tans, 1999). These differences represent a potential bias in the simulated $CO_2$ signal at, or downwind from, numerous locations associated with coastal/urban areas, and are the combined result of the differing emission distribution in the two experiments acted upon by the atmospheric transport.

### 3.3 Hourly $CO_2$ concentration

Here we examine the simulated $CO_2$ concentration differences at locations where $CO_2$ concentrations are directly monitored, in an attempt to provide more guidance to atmospheric $CO_2$ inversion studies that use these locations as the observational constraint to estimating carbon exchange between the ocean, land and atmosphere. An examination of the hourly time series of $CO_2$ concentration in the lowest model layer at GLOBALVIEW monitoring stations indicates that 169 stations (out of 313 total GLOBALVIEW stations) show hourly $CO_2$ concentration differences greater than ±0.10 ppm and 12 of these stations show differences that exceed ±2.0 ppm (Fig. 4). Most of the larger differences are located close to coastal urban areas and occur at night and the early morning hours. This is not surprising given the reduction in mixing between the free troposphere and the planetary boundary layer at these times.

The hourly differences at these 12 stations range from −32.1 ppm to +2.50 ppm. Tae-ahn Peninsula (TAP) has the largest response (−32.1 ppm) mainly due to its close proximity to a heavily populated coastal area and the subsequent large gradients in the experiment vs. control emissions. Yonagunijima (YON) and Gosan (GSN) also show





GMDD
7, 3575–3593, 2014



large responses, with maximum differences reaching +5.23 ppm and −4.43 ppm, respectively.

Given the fact that many atmospheric $CO_2$ inversions sample the simulated and observed $CO_2$ concentration as a local afternoon average, and the simulated maximum differences found here occur at varying times of day, greater insight can be gained by examining the simulated differences during the afternoon. In this case, 38 surface stations show hourly $CO_2$ concentration differences exceeding a magnitude of ±0.10 ppm during the local afternoon (12:00–18:00 LT). Of the 38 stations, five (TAP, GSN, SCSN, YON and RYO) have a local afternoon mean difference ranging between 0.12 ppm and −4.58 ppm (Fig. 4) with the largest difference at Tae-ahn Peninsula (TAP) in South Korea.

The shift between a positive and negative bias shown in Fig. 4 owes to the fact that these coastal sites likely experience onshore and offshore airflow at different times and this changes which portion of the local emission dipole influences the monitoring location. The specific circumstances at the TAP station are a good example of how the transport acts upon the emission dipoles to either enhance or diminish the concentration differences seen in Figs. 3 and 4. The TAP station is located approximately 300 m offshore in the Tae-ahn Peninsula and close to two large urban areas, Seosan and Hongseong, South Korea. The TAP monitoring station is located in the negative portion of the emission dipole displayed in Fig. 3 (emission difference = $-24.1\,\mathrm{Tg\,C\,gridcell^{-1}\,yr^{-1}}$), with the largest concentration difference (−32.1 ppm) occurring on 13 January at 5.00 p.m. PCTM wind fields show low wind speeds on 12 January (daily mean: $< 2\,\mathrm{m\,s^{-1}}$) and in the daytime of 13 January ($3.5\,\mathrm{m\,s^{-1}}$) compared to the much higher monthly mean value ($8.4\,\mathrm{m\,s^{-1}}$). The weak transport during this time period accentuates the difference between the two experiments by lessening the amount of horizontal mixing and dispersion of the dipole gradient in this location. Another feature to note is the seasonal pattern in the hourly $CO_2$ concentration difference time series, with larger absolute magnitudes appearing at RYO, YON and TAP in the spring and summer, indicating a seasonal contribution of atmospheric transport to the





GMDD
7, 3575–3593, 2014



potential monitoring station bias. Further examination of the hourly time series also shows diurnal patterns in all the monitoring sites shown here.

### 3.4 Implications for carbon cycle studies

Research in which simulated $CO_2$ concentrations are compared to observed must consider ways to avoid the potential bias introduced when regridding high-resolution fossil fuel $CO_2$ emissions to the lower-resolution grids typical of atmospheric transport models. Atmospheric $CO_2$ inversion studies are a good example of research that must overcome this potential problem. Utilizing the shuffling procedure outlined here is one way to minimize this potential bias in the spatial distribution of the fossil fuel $CO_2$ emissions. The goal is to maintain the localization of the large emission gradients that occur near coastlines due to the preponderance of large cities and point sources while simultaneously ensuring dynamic consistency between the emissions and modeled atmospheric transport.

Alternatively, modelers could use data selection procedures to minimize potential bias when choosing which $CO_2$ concentration observing sites to compare to simulated results (e. g., Law, 1996). Some inversion model system such as NOAA's CarbonTracker model sample only the afternoon daytime measurements at quasi-continuous stations to avoid times when the model boundary layer is less reliable (e.g. nighttime) (Peters et al., 2007). Eliminating or de-emphasizing (via the assignment of large uncertainty) atmospheric $CO_2$ monitoring locations that are near, or strongly influence by, large fossil fuel $CO_2$ sources can reduce the potential for the emissions regridding problem. However, given that many global carbon cycle studies are observationally underconstrained, this choice does come with potentially large information loss. Given this fact, we recommend the use of an emissions shuffling procedure.

Many earth system models avail of "tiling" techniques which can assign more than one surface characteristic to a gridcell. Without further research testing the sensitivity of results to this technique, it is unclear to what extent this minimizes the fossil fuel $CO_2$ emissions regridding problem discussed in this study.





GMDD
7, 3575–3593, 2014



## 4 Conclusions

This study tests the sensitivity of simulated $CO_2$ concentration to regridding of fossil fuel $CO_2$ emissions from a high resolution grid to a coarser global atmospheric transport model grid. Two experiments are conducted. The first regrids from the fine to coarse grid but with no post-regridding adjustment to those emitting gridcells that inevitably ends up in the ocean ("control"). The second experiment performs the same regridding process as (1) but moves or "shuffles" the ocean-based emissions to adjacent land gridcells in a proportional manner. The two experiments exhibit large fossil fuel $CO_2$ emissions differences in coastal regions, which range from $-30.3\,\mathrm{Tg\,C\,gridcell^{-1}\,yr^{-1}}$ ($-3.39\,\mathrm{kg\,C\,m^{-2}\,yr^{-1}}$) to $+30.0\,\mathrm{Tg\,C\,gridcell^{-1}\,yr^{-1}}$ ($+2.6\,\mathrm{kg\,C\,m^{-2}\,yr^{-1}}$) which, when summed globally, are equivalent to 10 % of the 2002 global total fossil fuel $CO_2$ emissions. After transport of these emissions through a global tracer transport model, these two experiments show simulated $CO_2$ concentration differences along the coastal margin in both the spatial and temporal domains. The resulting annual mean surface $CO_2$ concentration difference when examining all surface grid cells varies between $-6.60$ ppm to $+6.54$ ppm. At the hourly level, individual $CO_2$ concentration differences exceed $\pm 0.10$ ppm at 38 monitoring stations, with a maximum of $-32.1$ ppm at one monitoring locations. When examining local afternoon mean values (average of 12:00–18:00 LT), which both modeling systems and monitoring protocols emphasize, the $CO_2$ concentration differences are as large as $-4.58$ ppm. These $CO_2$ concentration differences result from the shifted emissions acted upon by modeled meteorology and can result in biased flux estimation in atmospheric $CO_2$ inversions which rely on comparison of simulated to measured $CO_2$. This phenomenon is also potentially important in any study investigating source-receptor simulations such as those found in air quality and other trace gas research efforts.





GMDD
7, 3575–3593, 2014



## Code availability

The Fortran code to regrid and reallocate the surface fossil fuel emissions flux to ensure the dynamical consistence between emission and global transport model is available from the corresponding author (email: Xia.Zhang11@asu.edu).

*Acknowledgements.* This work was supported by NASA CMS grant NNX12AP52G. Rayner is in receipt of an Australian Professorial Fellowship (DP1096309).

## References

Asefi-Najafabady, S., Rayner, P. J., Gurney, K. R., McRobert, A., Song, Y., Coltin, K., Elvidge, C., and Baugh, K.: A new global gridded dataset of $CO_2$ emissions from fossil fuel combustion: methodology, evaluation and analysis, J. Geophys. Res., in review, 2014.

Bosilovich, M. G.: Regional climate and variability of NASA MERRA and recent reanalyses: U. S. summertime precipitation and temperature, J. Appl. Meteorol. Clim., 52, 1939–1951, 2013.

Ciais, P., J., Paris, D., Marland, G., Peylin, P., Piao, S. L., Levin, I., Pregger, T., Scholz, Y., Friedrich, R., Rivier, L., Houwelling, S., Schulze, E. D., and members of the CARBOEUROPE Synthesis Team (1): The European carbon balance revisited, Part 4: fossil fuel emissions, Glob. Change Biol., 16, 1395–1408, doi:10.1111/j.1365-2486.2009.02098.x, 2011

Conway, T. J. and Tans, P. P.: Development of the $CO_2$ latitude gradient in recent decades, Global Biogeochem. Cy., 13, 821–826, 1999.

Elvidge, C. D., Ziskin, D., Baugh, K. E., Tuttle, B. T., Ghosh, T., Pack, D. W., Erwin, E. H., and Zhizhin, M.: A fifteen year record of global natural gas flaring derived from satellite data, Energies, 2, 595–622, 2009.

Enting, I.: Inverse Problems in Atmospheric Constituent Transport, Cambridge Univ. Press, New York, 2002.

Gurney, K. R., law, R. M., Denning, A. S., Rayner, P., Baker, D., Bousquet, P., Bruhwiler, L., Chen, Y., Ciais, P., Fan, S., Fung, I. Y., Gloor, M., Heimann, M., Higuchi, K., John, J., Maki, T., Maksyutov, S., Masarie, K, Peylin, P., Prather, M., Pak, B. C., Randerson, J., Sarmiento, J., Taguchi, S., Takahashi, T., and Yuen, C.: Towards robust regional estimates of $CO_2$ sources and sinks using atmospheric transport models, Nature, 415, 626–630, 2002.





GMDD

7, 3575–3593, 2014



Kawa, S. R., Erickson, D. J. III, Pawson, S., and Zhu, Z.: Global $CO_2$ transport simulations using meteorological data from the NASA data assimilation system, J. Geophys. Res., 109, D18312, doi:10.1029/2004JD004554, 2004.

Kawa, S. R., Mao, J., Abshire, J. B., Collatz, G., J., and Weaver, C. J.: Simulation studies for a space-based $CO_2$ lidar mission, Tellus, 62B, 759–769, 2010.

Law, R.: The selection of model-generated data $CO_2$ data: a case study with seasonal biospheric sources, Tellus B, 48, 474–486, 1996.

Le Quéré, C., Andres, R. J., Boden, T., Conway, T., Houghton, R. A., House, J. I., Marland, G., Peters, G. P., van der Werf, G. R., Ahlström, A., Andrew, R. M., Bopp, L., Canadell, J. G., Ciais, P., Doney, S. C., Enright, C., Friedlingstein, P., Huntingford, C., Jain, A. K., Jourdain, C., Kato, E., Keeling, R. F., Klein Goldewijk, K., Levis, S., Levy, P., Lomas, M., Poulter, B., Raupach, M. R., Schwinger, J., Sitch, S., Stocker, B. D., Viovy, N., Zaehle, S., and Zeng, N.: The global carbon budget 1959–2011, Earth Syst. Sci. Data, 5, 165–185, doi:10.5194/essd-5-165-2013, 2013.

Masarie, K. A. and Tans, P. P.: Extension and integration of atmospheric carbon dioxide data into a globally consistent measurement record, J. Geophys. Res., 100, 11593–11610, 1995.

Nassar, R., Napier-Linton, L., Gurney, K. R., Andres, R. J., Oda, T., Vogel, F. R., and Deng, F.: Improving the temporal and spatial distribution of $CO_2$ emissions from global fossil fuel emission data sets, J. Geophys. Res.: Atm, 118, 917–933, 2013.

Oda, T. and Maksyutov, S.: A very high-resolution (1 km × 1 km) global fossil fuel $CO_2$ emission inventory derived using a point source database and satellite observations of nighttime lights, Atmos. Chem. Phys., 11, 543–556, doi:10.5194/acp-11-543-2011, 2011.

Peters, W., Jacobson, A. R., Sweeney, C., Andrews, A. E., Conway, T. J., Masarle, K., Miller, J. B., Bruhwiler, L. M. P., Pétron, G., Hirsch, A. I., Worthy, D. E. J., vander Werf, G. R., Randerson, J. T., Wennberg, P. O., Krol, M. C., and Tans, P. P.: An atmospheric perspective on North American carbon dioxide exchange: CarbonTracker, P. Natl. Acad. Sci. USA,104, 18925–18930, 2007.

Peylin, P., Houweling, S., Krol, M. C., Karstens, U., Rödenbeck, C., Geels, C., Vermeulen, A., Badawy, B., Aulagnier, C., Pregger, T., Delage, F., Pieterse, G., Ciais, P., and Heimann, M.: Importance of fossil fuel emission uncertainties over Europe for $CO_2$ modeling: model intercomparison, Atmos. Chem. Phys., 11, 6607–6622, doi:10.5194/acp-11-6607-2011, 2011.





GMDD
7, 3575–3593, 2014



Rayner, P. J., Raupach, M. R., Paget, M., Peylin, P., and Koffi, E.: A new global gridded data set of $CO_2$ emissions from fossil fuel combustion: methodology and evaluation, J. Geophys. Res., 115, D19306, doi:10.1029/2009JD013439, 2010.

Wang, R., Tao, S., Ciais, P., Shen, H. Z., Huang, Y., Chen, H., Shen, G. F., Wang, B., Li, W., Zhang, Y. Y., Lu, Y., Zhu, D., Chen, Y. C., Liu, X. P., Wang, W. T., Wang, X. L., Liu, W. X., Li, B. G., and Piao, S. L.: High-resolution mapping of combustion processes and implications for $CO_2$ emissions, Atmos. Chem. Phys., 13, 5189–5203, doi:10.5194/acp-13-5189-2013, 2013.





GMDD
7, 3575–3593, 2014



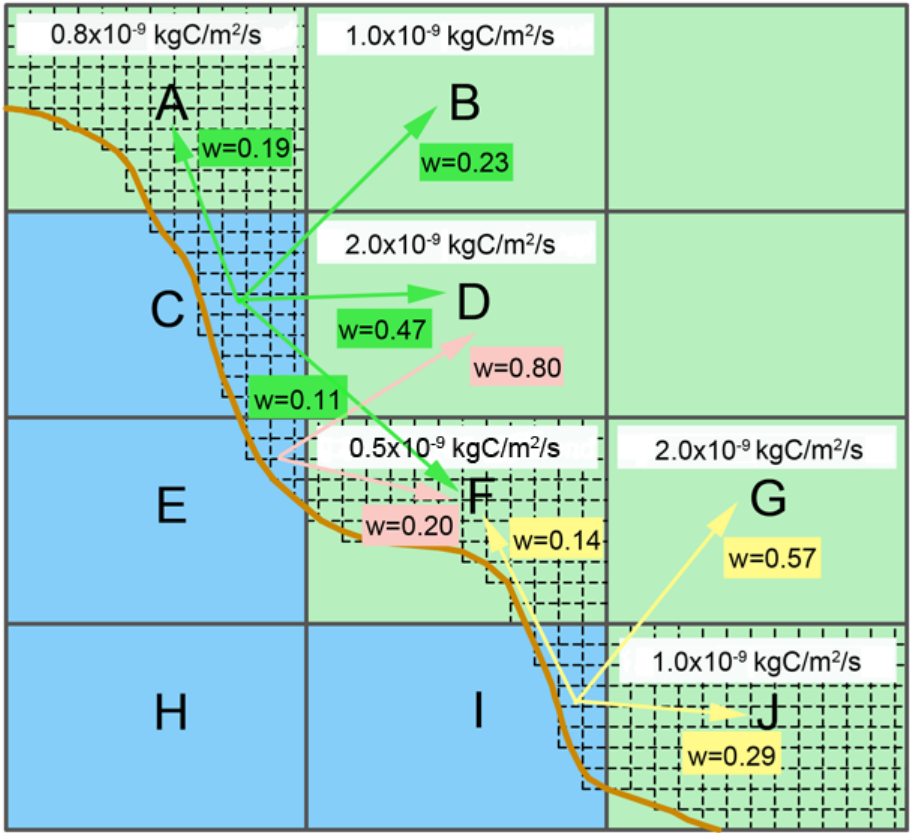


**Figure 1.** Depiction of the "shuffling" procedure when regridding from a 0.1° × 0.1° to a 1.25° × 1.0° model grid. Capital black letters denote the coarser model grid (1.25° × 1.0°). Gridcells outlined with dashed lines denote the finer model grid (0.1° × 0.1°). Green denotes land, blue denotes water. Example emission values and weighting values ($w$) and the direction of the allocation are included.





GMDD
7, 3575–3593, 2014



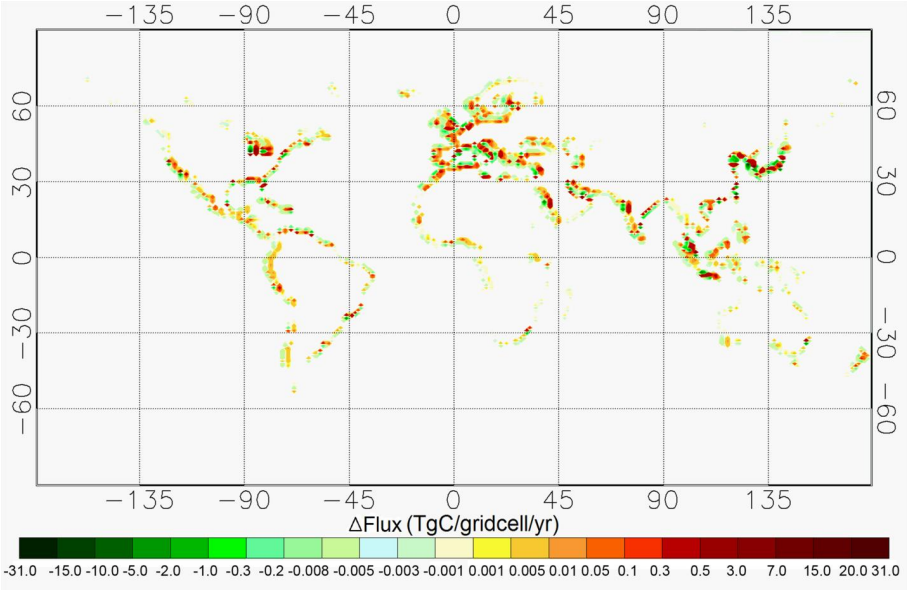


**Figure 2.** Difference between experiment and control fossil fuel $CO_2$ emissions. The difference is obtained by subtracting the control from the experiments.The emission values for some gridcells are not evident because the gridcells are saturated (beyond the color scale range). Units: Tg C gridcell$^{-1}$ yr$^{-1}$.





GMDD
7, 3575–3593, 2014



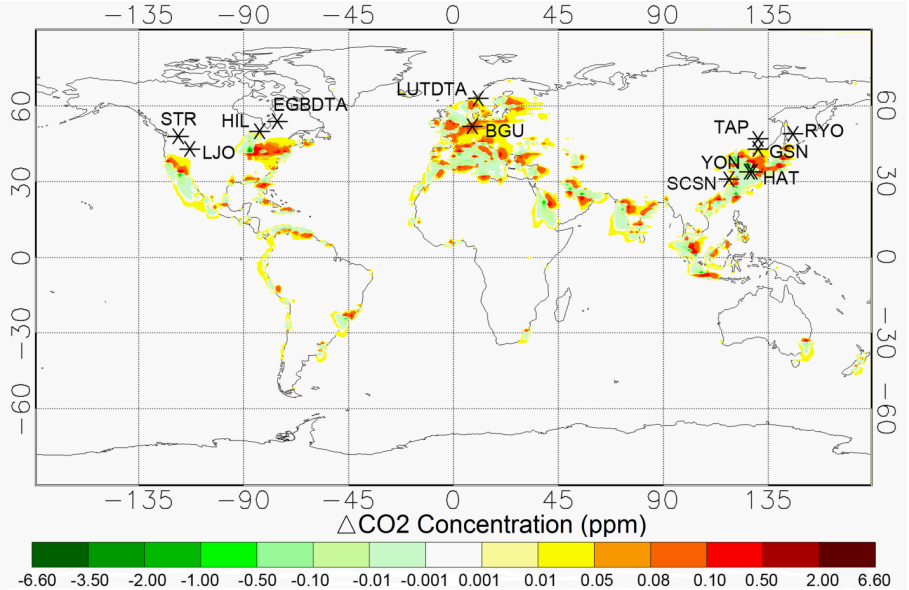


**Figure 3.** Simulated PCTM surface annual mean surface $CO_2$ concentration difference (control minus experiment, units: ppm). The * in the figure denotes existing $CO_2$ monitoring locations where the annual mean $CO_2$ concentration difference exceeds 2 ppm.





GMDD
7, 3575–3593, 2014



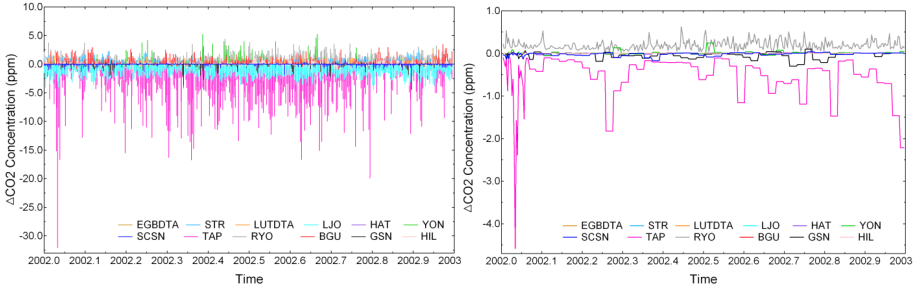


**Figure 4.** Simulated PCTM surface hourly $CO_2$ concentration difference (control minus experiment, units: ppm) at the 12 GLOBALVIEW monitoring stations with the largest concentration difference (left). Also shown are the local afternoon mean (12:00–18:00 LT) $CO_2$ concentration differences at the 12 stations (right).





GMDD
7, 3575–3593, 2014